Observation of Nuclear Scaling in the $A(e, e')$ Reaction at $x_B > 1$

K.Sh. Egiyan,[1] H.A. Bagdasaryan,[1] N.B. Dashyan,[1] M.M. Sargsian,[10] S.G. Stepanyan,[22] L.B. Weinstein,[22] G.S. Adams,[24] M.J. Amaryan,[1] E. Anciant,[26] M. Anghinolfi,[14] D.S. Armstrong,[7] B. Asavapibhop,[31] G.A. Asryan,[1] G. Audit,[26] T. Auger,[26] H. Avakian,[13] I.G. Aznauryan,[1] S. Barrow,[11] M. Battaglieri,[14] K. Beard,[17] M. Bektasoglu,[22] W. Bertozzi,[19] N. Bianchi,[13] A.S. Biselli,[24] S. Boiarinov,[15] B.E. Bonner,[25] D.Branford,[29] W.K. Brooks,[2] V.D. Burkert,[2] J.R. Calarco,[32] G.P. Capitani,[13] D.S. Carman,[21] B. Carnahan,[5] P.L. Cole,[36] A. Coleman,[7] D. Cords,[2] P. Corvisiero,[14] D. Crabb,[37] H. Crannell,[5] J. Cummings,[24] E. De Sanctis,[13] R. De Vita,[14] P.V. Degtyarenko,[2] R.A. Demirchyan,[1] H. Denizli,[33] L.C. Dennis,[11] A. Deppman,[13] K.V. Dharmawardane,[22] K.S. Dhuga,[12] C. Djalali,[35] G.E. Dodge,[22] D. Doughty,[6,2] P. Dragovitsch,[11] M. Dugger,[3] S. Dytman,[33] M. Eckhause,[7] Y.V. Efremenko,[15] H. Egiyan,[2] L. Elouadrhiri,[2] L. Farhi,[26] R.J. Feuerbach,[4] J. Ficenec,[38] K. Fissum,[19] T.A. Forest,[22] H. Funsten,[7] M. Gai,[28] G. Gavalian,[32] V.B. Gavrilov,[15] S. Gilad,[19] G.P. Gilfoyle,[34] K.L. Giovanetti,[17] P. Girard,[35] K.A. Griffioen,[7] M. Guidal,[16] M. Guillo,[35] V. Gyurjyan,[2] D. Hancock,[7] J. Hardie,[6] D. Heddle,[6,2] J. Heisenberg,[32] F.W. Hersman,[32] K. Hicks,[21] R.S. Hicks,[31] M. Holtrop,[32] C.E. Hyde-Wright,[22] W. Ingram,[30] M.M. Ito,[2] D. Jenkins,[38] K. Joo,[37] J.H. Kelley,[8] M. Khandaker,[20,2] K.Y. Kim,[33] W. Kim,[18] A. Klein,[22] F.J. Klein,[2,5] M. Klusman,[24] M. Kossov,[15] Y. Kuang,[7] S.E. Kuhn,[22] J.M. Laget,[26] D. Lawrence,[31] K. Loukachine,[38,5] M. Lucas,[35] R.W. Major,[34] J.J. Manak,[2] C. Marchand,[26] S. McAleer,[11] S.McLauchlen,[30] J.W.C. McNabb,[4] B.A. Mecking,[2] M.D. Mestayer,[2] C.A. Meyer,[4] K.Mikhailov,[15] R. Minehart,[37] M. Mirazita,[13] R. Miskimen,[31] V. Muccifora,[13] J. Mueller,[33] G.S. Mutchler,[25] J. Napolitano,[24] G. Niculescu,[21] B. Niczyporuk,[2] R.A. Niyazov,[22] M.S. Ohandjanyan,[1] A. Opper,[21] Y. Patois,[35] G.A. Peterson,[31] S. Philips,[12] N. Pivnyuk,[15] D. Pocanic,[37] O. Pogorelko,[15] E. Polli,[13] B.M. Preedom,[35] J.W. Price,[27] D. Protopopescu,[32] L.M. Qin,[22] B.A. Raue,[10,2] A.R. Reolon,[13] G. Riccardi,[11] G. Ricco,[14] M. Ripani,[14] B.G. Ritchie,[3] F. Ronchetti,[13] P. Rossi,[13] D. Rowntree,[19] P.D. Rubin,[34] C.W. Salgado,[20] M. Sanzone,[13] V. Sapunenko,[14] R.A. Schumacher,[4] Y.G. Sharabian,[2] J. Shaw,[31] S.M. Shuvalov,[15] A. Skabelin,[19] E.S. Smith,[2] L.C. Smith,[37] T. Smith,[32] D.I. Sober,[5] M. Spraker,[8] A. Stavinskiy,[15] P. Stoler,[24] M. Strikman,[23] R. Sulaman,[19] M. Taiuti,[14] S. Taylor,[25] D. Tedeschi,[35] R. Thompson,[33] L. Todor,[4] T.Y. Tung,[7] M.F. Vineyard,[34] A. Vlassov,[15] H. Weller,[8] R. Welsh,[7] D.P. Weygand,[2] S. Whisnant,[35] M. Witkowski,[24] E. Wolin,[2] A. Yegneswaran,[2] J. Yun,[22] B. Zhang,[19] Z. Zhou,[19] and J. Zhao[19]

(The CLAS Collaboration)

[1]*Yerevan Physics Institute, 375036 Yerevan, Armenia*
[2]*Thomas Jefferson National Accelerator Facility, 12000 Jefferson Avenue, Newport News, VA 23606, USA*
[3]*Arizona State University, Department of Physics and Astronomy, Tempe, AZ 85287, USA*
[4]*Carnegie Mellon University, Department of Physics, Pittsburgh, PA 15213, USA*
[5]*Catholic University of America, Department of Physics, Washington D.C., 20064, USA*
[6]*Christopher Newport University, Newport News, VA 23606, USA*
[7]*College of William and Mary, Department of Physics, Williamsburg, VA 23187, USA*
[8]*Duke University, Physics Bldg. TUNL, Durham, NC27706, USA*
[9]*Department of Physics and Astronomy, Edinburgh University, Edinburgh EH9 3JZ, United Kingdom*
[10]*Florida International University, Miami, FL 33199, USA*
[11]*Florida State University, Department of Physics, Tallahassee, FL 32306, USA*
[12]*George Washington University, Department of Physics, Washington D. C., 20052 USA*
[13]*Istituto Nazionale di Fisica Nucleare, Laboratori Nazionali di Frascati, P.O. 13, 00044 Frascati, Italy*
[14]*Istituto Nazionale di Fisica Nucleare, Sezione di Genova, Dipartimento di Fisica dell'Universita, 16146 Genova, Italy*
[15]*Institute of Theoretical and Experimental Physics, 25 B. Cheremushkinskaya, Moscow, 117259, Russia*
[16]*Institut de Physique Nucleaire d'Orsay, IN2P3, BP 1, 91406 Orsay, France*
[17]*James Madison University, Department of Physics, Harrisonburg, VA 22807, USA*
[18]*Kyungpook National University, Department of Physics, Taegu 702-701, South Korea*
[19]*Massachusetts Institute of Technology, Cambridge, MA 02139, USA"*
[20]*Norfolk State University, Norfolk VA 23504, USA*
[21]*Ohio University, Department of Physics, Athens, OH 45701, USA*
[22]*Old Dominion University, Department of Physics, Norfolk VA 23529, USA*
[23]*Pennsylvania State University, Department of Physics, State Collage, Pennsylvania 16802, USA*
[24]*Rensselaer Polytechnic Institute, Department of Physics, Troy, NY 12181, USA*
[25]*Rice University, Bonner Lab, Box 1892, Houston, TX 77251, USA*
[26]*CEA Saclay, DAPNIA-SPhN, F91191 Gif-sur-Yvette Cedex, France*
[27]*University of California at Los Angeles, Department of Physics and Astonomy, Los Angeles, CA 90095-1547, USA*

[28] University of Connecticut, Physics Department, Storrs, CT 06269, USA
[29] University of Edinburg, Department of Physics and Astronomy, Edinburgh EH9 3JZ, Scotland, UK
[30] University of Glasgow, Glasgow, G12 8QQ, Scotland, UK
[31] University of Massachusetts, Department of Physics, Amherst, MA 01003, USA
[32] University of New Hampshire, Department of Physics, Durham, NH 03824, USA
[33] University of Pittsburgh, Department of Physics and Astronomy, Pittsburgh, PA 15260, USA
[34] University of Richmond, Department of Physics, Richmond, VA 23173, USA
[35] University of South Carolina, Department of Physics, Columbia, SC 29208, USA
[36] University of Texas at El Paso, Department of Physics, El Paso, Texas 79968, USA
[37] University of Virginia, Department of Physics, Charlottesville, VA 22903, USA
[38] Virginia Polytechnic and State University, Department of Physics, Blacksburg, VA 24061, USA
(Dated: December 16, 2002)

The ratios of inclusive electron scattering cross sections of ^{4}He, ^{12}C, and ^{56}Fe to ^{3}He have been measured for the first time. It is shown that these ratios are independent of x_B at $Q^2 > 1.4$ (GeV/c)^2 for $x_B > 1.5$ where the inclusive cross section depends primarily on the high momentum components of the nuclear wave function. This scaling was predicted by the Short Range Correlation (SRC) model. The values of these ratios in the scaling region are related to the relative probabilities of SRC in these nuclei. Our data demonstrate that for nuclei with $A \geq 12$ these probabilities are about 5 times larger than in deuterium, while for ^{4}He it is larger by a factor of only about 3.

PACS numbers: PACS : 13.60.Le, 13.40.Gp, 14.20.Gk

I. INTRODUCTION

Due to the strong interaction and short distances between the nucleons in nuclei, there is a noticeable probability for nucleon wave functions to overlap, resulting in short range nucleon-nucleon correlations (SRC) in nuclei [1]. Investigation of SRC is important for at least two reasons. First, because of the short range nature of these correlations, they should contribute significantly to the high momentum component of the nuclear wave function. Second, scattering from SRC will provide unique data on the modification of deeply bound nucleons, which is extremely important for a complete understanding of nucleon structure in general.

High energy inclusive electron scattering from nuclei, $A(e,e')$, is one of the simplest ways to investigate SRC. In particular, it is probably the best way to measure the probabilities of SRC in nuclei. The main problem in these studies is selecting the electron-SRC scattering events from the orders-of-magnitude larger background of inelastic and/or quasi-elastic interaction of electrons with the uncorrelated low momentum nucleons.

By measuring cross sections at

$$x_B = \frac{Q^2}{2M\nu} > 1, \tag{1}$$

where Q^2 is the negative four momentum squared of the virtual photon ($Q^2 = -q^\mu q_\mu > 0$), ν is the energy transfer, x_B is the Bjorken scaling variable, and M is the nucleon mass, contributions from inelastic electron-nucleon scattering and meson exchange currents (at high Q^2) can be significantly reduced. This corresponds to studying the low energy loss side of the quasi-elastic peak.

Many previous analyzes of data in this kinematic region concentrate on using y-scaling to study nucleon momentum distributions (see [2] and references there in). While this technique provides some information about the nuclear wave function, it does not measure the probability of finding SRC in nuclei.

Meanwhile, the data at $x_B > 1$ can be used to measure the probability of finding SRC in nuclei. There are theoretical predictions that at momenta higher than the Fermi momentum (e.g. $p_m > 0.35$ GeV/c), the nucleon momentum distributions in light and heavy nuclei are similar (see e.g. [3]). This implies that they originate predominantly from the interaction between two nearby nucleons, *i.e.* due to SRC. If the $A(e,e')$ cross section depends primarily on the nuclear wave function and the shape of this wave function at high momentum is really universal, then in this high momentum region the ratio of weighted[32] (e,e') cross sections for different nuclei should scale, *i.e.* they should be independent of electron scattering variables (Q^2 and x_B), with the magnitude of the scaling factor being proportional to the relative probability of SRC in the two nuclei [4, 5].

In Ref. [5] this was checked by analyzing existing SLAC $A(e,e')$ data for deuterium [6–8] and heavier nuclei [9]. They found an indication of scaling at $Q^2 > 1$ and $x \geq 1.5$. However, since the data for deuterium and the heavy nuclei were collected in different experiments at similar Q^2 but at different electron scattering angles and incident electron energies, to find the ratios at the same values of (x_B, Q^2), a complicated fitting and interpolation procedure was applied [5] to the data. The main problem was that the cross sections varied very strongly with angle, incident energy, and Q^2. To simplify the interpolation, the electron-deuteron cross section was first divided by the theoretical calculation within the impulse approximation. Therefore, the data are not purely experimental, since they include the theoretical calculations, and the ratios may have been affected by the fitting and interpolation procedures.

In this work, the yields of the reaction $A(e,e')$ for ^{3}He,

^{4}He, ^{12}C and ^{56}Fe targets are measured in the same kinematical conditions, and the ratios $A(e,e')/{}^3\mathrm{He}(e,e')$ are obtained for $1 < x_B < 2$ and $Q^2 > 0.65$ (GeV/c)^2. Furthermore, using the scaling behavior of these ratios, predicted in [4, 5], the relative probability of NN SRC for the various nuclei have been extracted.

II. KINEMATICS AND PREDICTIONS

In order to suppress the background from quasi-elastic interactions of electrons with the uncorrelated low momentum nucleons (see Fig. 1a), we further restrict the kinematic variables x_B and Q^2.

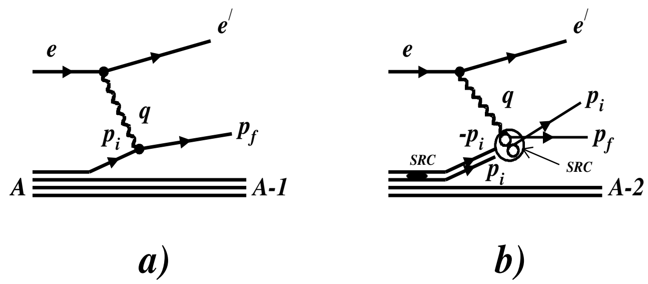

FIG. 1: Two mechanisms of $A(e,e')$ scattering. a) single nucleon model; b) Short Range Correlation model.

For quasi-elastic $A(e,e')$ scattering, x_B, Q^2, and the minimum $A-1$ recoil momentum contributing to the reaction, are related by energy and momentum conservation:

$$(q + p_A - p_{A-1})^2 = p_f^2 = m_N^2, \tag{2}$$

where q, p_A, p_{A-1}, and p_f are the four momenta of the virtual photon, target nucleus, residual $A-1$ system, and knocked-out nucleon respectively (note that only q and p_A are measured.) From Eq.(2) one obtains:

$$\Delta M^2 - Q^2 + \frac{Q^2}{m_N x_B}\left(M_A - \sqrt{M_{A-1}^2 + \vec{p}_m{}^2}\right)$$
$$-2\vec{q}\cdot\vec{p}_m - 2M_A\sqrt{M_{A-1}^2 + \vec{p}_m{}^2} \;=\; 0, \tag{3}$$

where $\Delta M^2 = M_A^2 + M_{A-1}^2 - m_N^2$ and $\vec{p}_m = \vec{p}_f - \vec{q} = -\vec{p}_{A-1}$ is the recoil momentum involved in the reaction (sometimes referred to as the 'missing momentum' in $(e,e'p)$ reactions). Eq. (3) defines a simple relationship between $|\vec{p}_m{}^{min}|$ and x_B at fixed Q^2. This relation for deuterium at various values of Q^2 is shown in Fig. 2a. Fig. 2b shows the same relationship for various nuclei at $Q^2 = 2$ (GeV/c)^2. Note that this relationship is different for the different nuclei, due primarily to differences in the mass of the recoil $A-1$ system. This minimum recoil momentum is one of the possible definitions of the scaling variable y.

One can see from Fig. 2 that for any nucleus A and fixed Q^2, we can find the value x_B^o such that at $x_B > x_B^o$ the magnitude of the minimum recoil momentum, $|\vec{p}_m{}^{min}|$, contributing to the reaction, exceeds the average Fermi momentum in nucleus A.

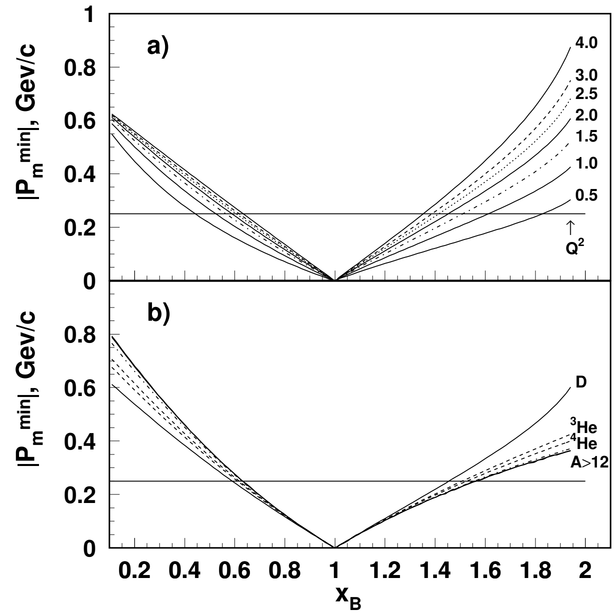

FIG. 2: The minimum recoil momentum as a function of x_B. a) For deuterium at several Q^2 (in (GeV/c)^2); b) For different nuclei at $Q^2 = 2.0$ (GeV/c)^2. Horizontal lines at 250 MeV/c indicate the Fermi momentum typical of the uncorrelated motion of nucleons in nuclei.

It should be pointed out that only in the simplest model, where the virtual photon is absorbed on one nucleon and that nucleon leaves the nucleus without further interactions (the Plane Wave Impulse Approximation), the initial momentum of the struck nucleon is just $\vec{p}_i = \vec{p}_m$. In reality, the (e,e') reaction effectively integrates over many values of $p_m \geq p_m^{min}$. In addition, this simple relation between recoil momentum and initial momentum is modified by Final State Interactions (FSI) and the excitation energy of the residual nucleus. These make it difficult to determine the nuclear wave function directly from (e,e') cross sections. However, for our purposes, it is sufficient to know that when the minimum recoil momentum contributing to the reaction is much larger than the Fermi momentum, the initial momentum of the struck nucleon will also be larger.

Let us now consider various predictions of the ratios of weighted (e,e') cross sections for different nuclei. In the mechanism for inclusive (e,e') scattering at $x > 1$ with virtual photon absorption on a single nucleon and the $A-1$ system recoiling intact without FSI (see Fig. 1a), the minimum recoil momentum for different nuclei at fixed Q^2 differs and this difference increases with x_B (see Fig. 2). Therefore, the cross section ratio between different nuclei will increase with x_B and will not scale.

In the Short-Range Correlations model of Frankfurt and Strikman [1] (see Fig. 1b) the high momentum part of the nuclear momentum distribution is due to correlated nucleon pairs. This means that when the electron scatters from a high-momentum nucleon in the nucleus, we can consider this scattering as an electron-deuterium interaction with the spectator $A-2$ system almost at rest. Therefore, according to Fig. 2a, starting from some threshold x_B^0 for fixed Q^2 the cross section ratio

$$R_{A2}^{A1}(Q^2, x_B) = \frac{\sigma_{A_1}(Q^2, x_B)/A_1}{\sigma_{A_2}(Q^2, x_B)/A_2}, \tag{4}$$

where σ_{A_1} and σ_{A_2} are the inclusive electron scattering cross sections from nuclei with atomic numbers A_1 and A_2 respectively, will scale (will be constant). Scaling results from the dominance of SRC in the high momentum component of the nuclear wave function, and it should be observed, for example, for the cross section ratios of heavy nuclei to light nuclei such as ^{3}He.

Fig. 3a shows $R^C_{^3He}$, for $A_1 = {}^{12}$C and $A_2 = {}^3$He, as a function of x_B for Q^2 from 1.5 to 2.5 (GeV/c)^2 calculated in the SRC model [10]. The ratio for $A_1 = {}^{56}$Fe and $A_2 = {}^3$He is shown in Fig. 3b. The calculations used the Faddeev wave function for ^{3}He calculated using the Bonn NN potential. The momentum distributions for heavier nuclei have been modeled through a two-component momentum distribution using mean field distributions for small nucleon momenta and using the deuteron momentum distribution for $p > 300$ MeV/c, scaled by factor $a_2(A)$, per-nucleon probability of NN SRC in nucleus A, estimated from [5]. The mean field momentum distributions used the Harmonic Oscillator wave function for ^{12}C and the Quasi-particle Lagrange Method of [11] for ^{56}Fe. For the description of the eN interaction, the Bodek nucleon inelastic form-factor parameterization [12], and the dipole elastic form-factors have been used. These calculations are in reasonable agreement with existing $A(e,e')X$ experimental data from SLAC [13] and from Jefferson Lab Hall C [14].

The ratios in Fig. 3 show a nice plateau starting from $x_B > 1.5$ for both nuclei and all Q^2. The experimentally obtained ratio in the scaling region can be used to determine the relative probability of finding correlated NN pairs in different nuclei. However one needs to take into account two main factors: first the final state interactions (FSI) of a nucleon with the residual system, and second the NN pair center of mass motion.

In the SRC model, FSI do not destroy the scaling behavior of the ratio, R. Indeed, in the light-cone approximation of the SRC model, if the invariant mass of the final NN system is sufficiently large, $\sqrt{(q+m_D)^2} - m_D > 50 - 100$ MeV, then the scattering amplitude will depend mainly on the light-cone fraction of the interacting nucleon's momentum $\alpha = (E - p_z)/M$, and has only a weak dependence on the conjugated variables $E + p_z$ and p_t [5, 15, 16]. As a result, the closure approximation can be applied in the light-cone reference frame, and the inclusive cross section will depend on the light-cone momentum distribution of the nucleon in the nucleus, integrated over the transverse momentum of the nucleon, $\rho_A(\alpha)$. Thus, within light cone description the Eq.(4) measures the ratio of $\rho_A(\alpha)$ for nuclei A_1 and A_2 in the high momentum range of the target nucleon.

In the lab frame description (in the virtual nucleon approach), however, the closure approximation can not be applied for large values of interacting nucleon momenta, and FSI should be calculated explicitly (see e.g. [15]). Within the SRC model at high recoil momenta, FSI are dominated by the rescattering of the knocked-out nucleon with the correlated nucleon in the SRC [5, 15]. Therefore, FSI will be localized in SRC, and will cancel in the ratio R. As a result, Eq.(4) at $x_B > x_B^0$ could be related to the ratio of momentum distributions of nuclei A_1 and A_2 with the momentum which does not coincide with $\vec{p}_m$ but still is larger than characteristic Fermi momentum of the nuclei [15].

Having an underlying model of the nuclear spectral function, one can relate the measured ratios in Eq.(4) to the SRC properties of the nuclear wave function. Within the spectral function model[1], in which two nucleon SRC is assumed at rest with the high momentum distribution identical to that of deuteron wave function, the ratio in Eq.(4) could be directly related to the per-nucleon SRC probability in nucleus A relative to deuterium, $a_2(A)$. In models of the nuclear spectral function [17] in which two nucleon correlations are moving in the mean field of the spectator $A-2$ system, the analysis of Eq. (4) will yield slightly smaller values for $a_2(A)$. Calculations by Ciofi degli Atti [18] indicate that this motion does not affect the scaling but can decrease the extracted $a_2(A)$ for ^{56}Fe by up to 20%. However it is important to emphasize that since both approximations predict similar (light cone) momentum distributions, both models lead to a similar ratio of the light-cone spectral functions and the overall probability of high momentum nucleons remains practically the same.

One can summarize the predictions of the SRC model for the ratios of the inclusive cross sections from different nuclei as follows (see Fig. 3):

- Scaling (x_B independence) is expected at $Q^2 \geq 1$ GeV^2 for $x_B^0 \leq x_B < 2$ where x_B^0 is the threshold for high recoil momentum.
- No scaling is expected at $Q^2 < 1$ (GeV/c)^2.
- For $x_B \leq x_B^0$ the ratios should have a minimum at $x_B = 1$ and should grow with x_B since heavy nuclei have broader momentum distribution than light nuclei for $p < 0.3$ GeV/c.
- The onset of scaling depends on Q^2; x_B^0 should decrease with increasing Q^2.
- In the scaling regime, the ratios should be independent of Q^2.
- In the scaling regime the ratios should depend only weakly on A for $A \geq 10$. This reflects nuclear saturation.

- Ratios in the scaling regime are proportional to the relative probability of two-nucleon SRC in the two nuclei.

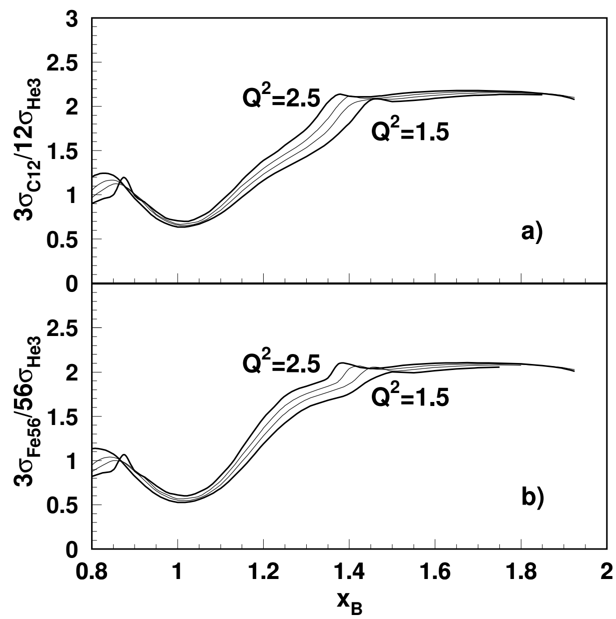

FIG. 3: SRC Model predictions for the normalized inclusive cross section ratio as a function of x_B for several values of Q^2 (in (GeV/c)^2). Note the scaling behavior predicted for $x_B > 1.4$. a) ^{12}C to ^{3}He, b) ^{56}Fe to ^{3}He.

Another possible mechanism for inclusive (e, e') scattering at $x_B > 1$ is virtual photon absorption on a single nucleon followed by NN rescattering [19, 20]. Benhar *et al.* use the nuclear spectral function in the lab system and calculate the FSI using a correlated Glauber approximation (CGA), in which the initial momenta of the rescattered nucleons are neglected. In this model the cross section at $x > 1$ originates mainly from FSI and therefore the cross section ratios will not scale. This model predicts that these ratios also depend on Q^2, since it includes a noticeable reduction of FSI in order to agree with the data at $Q^2 \geq 2$ (GeV/c)^2. Benhar *et al.* attribute this reduction in FSI to color transparency effects [33]. The requirement of large color transparency effects also results in a strong A dependence of the ratio since the amount of the FSI suppression depends on the number of nucleons participating in rescattering.

The main predictions of the CGA model for the nuclear cross section ratios are as follows:

- No scaling is predicted for $Q^2 \geq 1$ (GeV/c)^2 and $x_B < 2$.
- The nuclear ratios should vary with Q^2.
- The ratios should depend on A.
- The model is not applicable below $Q^2 = 1$ (GeV/c)^2.

Thus, measuring the ratios of inclusive (e, e') scattering at $x_B > 1$ and $Q^2 > 1$ (GeV/c)^2 will yield important information about the reaction dynamics. If scaling is observed, then the dominance of the SRC in the nuclear wave function is manifested and the measured ratios will contain information about the probability of two nucleon short range correlations in nuclei.

III. EXPERIMENT

In this paper we present the first experimental studies of ratios of normalized, and acceptance and radiative corrected, inclusive yields of electrons scattered from ^{4}He, ^{12}C, ^{56}Fe, and ^{3}He measured under identical experimental conditions.

The measurements were performed with the CEBAF Large Acceptance Spectrometer (CLAS) in Hall B at the Thomas Jefferson National Accelerator Facility. This is the first CLAS experiment with nuclear targets. Electrons with 2.261 and 4.461 GeV energies incident on ^{3}He, ^{4}He, ^{12}C, and ^{56}Fe targets have been used. We used helium liquefied in cylindrical target cells 1 cm in diameter and 4 cm long, positioned on the beam approximately in the CLAS center. The solid targets were thin foils of ^{12}C (1mm) and ^{56}Fe (0.15 mm) positioned 1.5 cm downstream of liquid target exit window. Data on solid targets have been taken with empty liquid target cell. The CLAS detector [22] consists of six sectors, each functioning as an independent magnetic spectrometer. Six superconducting coils generate a toroidal magnetic field primarily in the azimuthal direction. Each sector is instrumented with multi-wire drift chambers [23] and time-of-flight scintillator counters [24] that cover the angular range from 8^o to 143^o, and, in the forward region ($8^o < \theta < 45^o$), with gas filled threshold Cherenkov counters (CC) [25] and lead-scintillator sandwich-type electromagnetic calorimeters (EC) [26]. Azimuthal coverage for CLAS is limited only by the magnetic coils, and is approximately 90% at large polar angles and 50% at forward angles. The CLAS was triggered on scattered electrons by a CC-EC coincidence at 2.2 GeV, and by the EC alone with a ≈ 1 GeV electron threshold at 4.4 GeV.

For our analysis, electrons are selected in the kinematical region $Q^2 > 0.65$ (GeV/c)^2 and $x_B > 1$ where the contribution from the high momentum components of the nuclear wave function should be enhanced. We also require that the energy transfer, ν, should be > 300 MeV (the characteristic missing energy for SRC ~ 260 MeV [1]). In this region one expects that inclusive $A(e, e')$ scattering will proceed through the interaction of the incoming electron with a correlated nucleon in an SRC.

A. Electron Identification

Electrons were selected in the fiducial region of the CLAS sectors. The fiducial region is a region of azimuthal

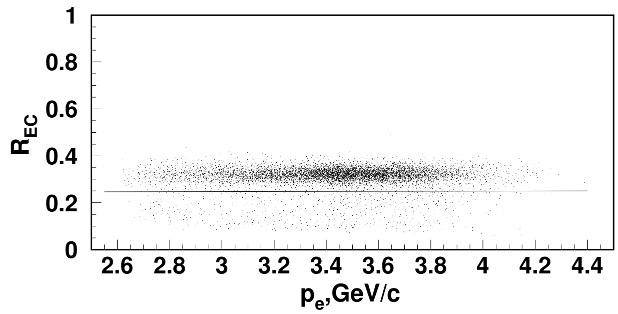

FIG. 4: The ratio (R_{EC}) of energy deposited in the CLAS electromagnetic calorimeter (EC) to the electron momentum p_e as a function of p_e at beam energy 4.461 GeV. The lines at $R_{EC} \approx 0.25$ are located 3 standard deviations below the mean, as determined by measurements at several values of p_e. This cut was used to identify electrons.

angle, for given momentum and polar angle, where the electron detection efficiency is constant. Then a cut on the ratio of the energy deposited in the EC to the measured electron momentum p_e (R_{EC}) was used for final selection. In Fig. 4 R_{EC} vs. p_e for the ^{56}Fe target at 4.4 GeV is shown. The lines show the applied cut at $R_{EC} \approx 0.25$ which is located 3 standard deviations below the mean as determined by measurements at several values of p_e. A Monte Carlo simulation showed that these cuts reduce the $A(e, e')$ yield by less then 0.5%.

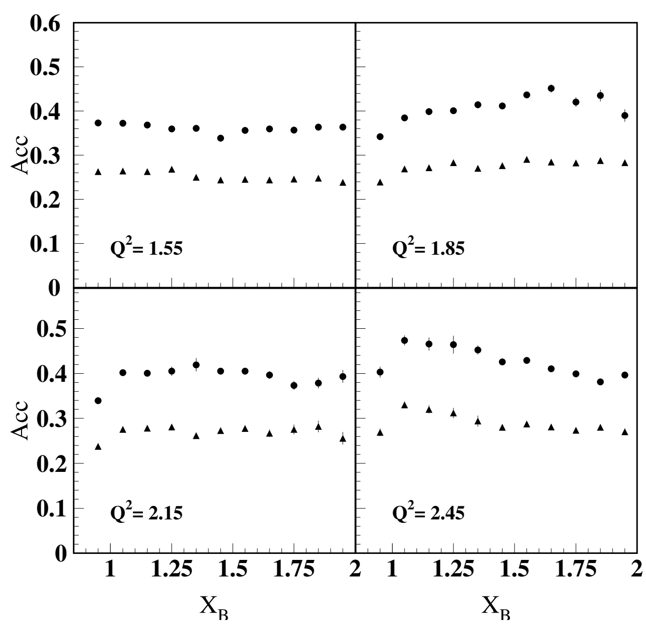

FIG. 5: The acceptance correction factors as a function of x_B. • ^{3}He, ▲ ^{12}C. Q^2 are in (GeV/c)^2.

We estimated the π^- contamination in the electron sample for a wide angular range using the photo-electron distributions in the CLAS Cherenkov counters. We found that for $x_B > 1$ this is negligible.

B. Acceptance Corrections

We used Monte Carlo technique to determine the electron acceptance correction factors. Two iterations were done to optimize the cross section model for this purpose. In the first iteration we generated events using the SRC model [10] and determined the CLAS detector response using the GEANT-based CLAS simulation program, taking into account "bad" or "dead" hardware channels in various components of CLAS, as well as realistic position resolution for CLAS drift chambers. We then used the CLAS data analysis package to reconstruct these events using the same electron identification criteria that was applied to the real data. The acceptance correction factors were found as the ratios of the number of simulated and reconstructed events in each kinematic bin. Then the acceptance corrections were applied to the data event-by-event, i.e. each event was weighted by the acceptance factor obtained for the corresponding $(\Delta x_B, \Delta Q^2)$ kinematic bin and the cross sections were calculated as a function of x_B and Q^2. For the second iteration the obtained cross sections were fitted and the fit-functions were used to generate a new set of data, and the process was repeated again. Fig. 5 shows the electron acceptance factors after the second iteration for liquid (^{3}He) and solid (^{12}C) targets. We used the difference between the iterations as the uncertainty in the acceptance correction factor. Note that the acceptance for the carbon target is smaller then for the helium target. This is due to the closer location of the solid targets to the CLAS coils, that limit azimuthal angular coverage of the detectors.

C. Radiative Corrections

The cross section ratios were corrected for radiative effects. The radiative correction for each target as a function of Q^2 and x_B was calculated as the ratio

$$C_{rad}(x_B, Q^2) = \frac{d\sigma^{rad}(x_B, Q^2)}{d\sigma^{norad}(x_B, Q^2)}, \tag{5}$$

where $d\sigma^{rad}(x_B, Q^2)$ and $d\sigma^{norad}(x_B, Q^2)$ are the radiatively corrected and uncorrected theoretical cross sections, respectively. The cross sections have been calculated using [10].

IV. RESULTS

We constructed ratios of normalized, acceptance and radiative corrected inclusive electron yields on nuclei ^{4}He, ^{12}C and ^{56}Fe over the yield on ^{3}He in the range of kinematics $1 < x_B < 2$. Assuming that electron detection

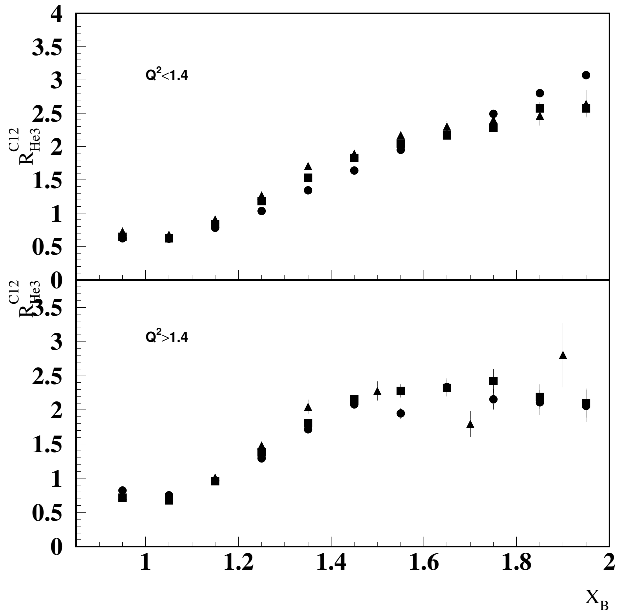

FIG. 6: $R^C_{^3He}$, the per-nucleon yield ratios for C to ^{3}He. a) • 0.65< Q^2 < 0.85; ■ 0.9< Q^2 < 1.1; ▲ 1.15< Q^2 < 1.35 $(\mathrm{GeV/c})^2$, all at incident energy 2.261 GeV.
b) • 1.4< Q^2 < 1.6 $(\mathrm{GeV/c})^2$ and at incident energy 2.261 GeV; ■ 1.4< Q^2 < 2.0 ; ▲ 2.0< Q^2 < 2.6 $(\mathrm{GeV/c})^2$, both at incident energy 4.461 GeV.

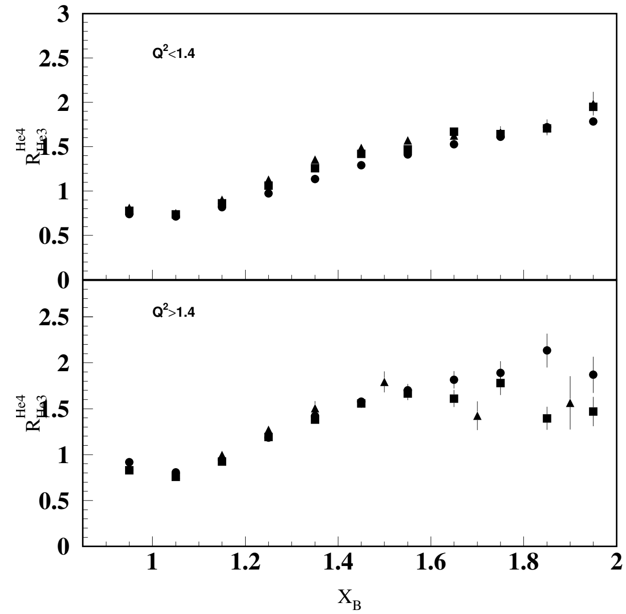

FIG. 7: The same as Fig. 6 for ^{4}He.

efficiency from different targets are the same, these ratios, weighted by atomic number, are equivalent to the ratios of cross sections in Eq. 4.

The normalized yields for each x_B and Q^2 bin have been calculated as:

$$\frac{d\mathcal{Y}}{dQ^2 dx_B} = \frac{N_{e'}}{\Delta Q^2 \Delta x_B N_e N_T} \cdot \frac{1}{Acc} \tag{6}$$

where $N_{e'}$, N_e and N_T are the number of scattered electrons, incident electrons and target nuclei, respectively. Acc is the acceptance correction, and ΔQ^2 and Δx_B are the bin sizes in Q^2 and in x_B, respectively. Since electron detection efficiency in CLAS is expected to be > 0.96, we compare obtained yields with radiated cross sections calculated by [10]. At this level satisfactory agreement has been found between our results and the calculations from [10] that were tuned on SLAC [13] and Jefferson Lab Hall C [14] data.

The ratios $R^A_{^3He}$, also corrected for radiative effects, are defined as:

$$R^A_{^3He}(x_B) = \frac{3d\mathcal{Y}^{\mathcal{A}}}{Ad\mathcal{Y}^{^3He}} \frac{C^A_{Rad}}{C^{^3He}_{Rad}} \tag{7}$$

where $\mathcal{Y}$ is the normalized yield, Eq. 6, and C_{Rad} is the radiative correction factor from Eq. 5 for each nucleus.

Fig. 6 shows these ratios for ^{12}C at several values of Q^2. Figs. 7 and 8 show these ratios for ^{4}He and ^{56}Fe, respectively. These data have the following important characteristics:

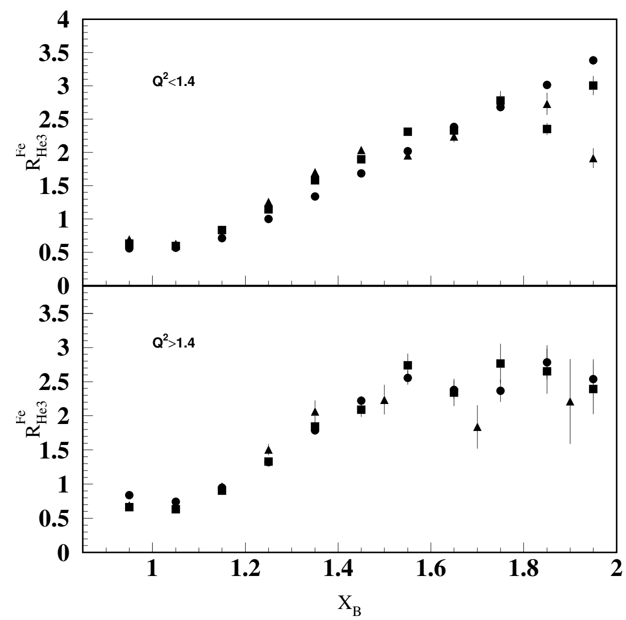

FIG. 8: The same as Fig. 6 for ^{56}Fe.

- There is a clear Q^2 evolution of the ratio's shape:
  - At low Q^2 ($Q^2 < 1.4$ $(\mathrm{GeV/c})^2$), $R^A_{^3He}(x_B)$ increases with x_B in the entire $1 < x_B < 2$ range (see Figs. 6a – 8a).
  - At high Q^2 ($Q^2 \geq 1.4$ $(\mathrm{GeV/c})^2$) $R^A_{^3He}(x_B)$ is independent of x_B for $x_B > x^0_B \approx 1.5$. (See Figs. 6b – 8b.)
- The value of $R^A_{^3He}(x_B)$ in the scaling regime is independent of Q^2.

- The value of $R^A_{^3He}(x_B)$ in the scaling regime for $A > 10$ suggests a weak dependence on target mass.

A. Systematic Errors

The systematic errors in this measurement are different for different targets and include uncertainties in:

- fiducial cut applied: $\approx 1\%$;
- radiative correction factors: $\approx 2\%$;
- target densities and thicknesses: $\approx 0.5\%$ and 1.0% for solid targets; 0.5% and 3.5% for liquid targets respectively.
- acceptance correction factors (Q^2 dependent): between 2.2 and 4.0% for solid targets and between 1.8 and 4.3% for liquid targets.

In the ratios of yields from two targets, some of them will cancel out. For the ^{3}He/^{4}He ratio, all but uncertainties on the beam current and the target density divide out, giving a total systematic uncertainty of 0.7%.

For the solid-target to ^{3}He ratios, only the electron detection efficiency cancels. The quadratic sum of the other uncertainties is between 5% and 7%, depending on Q^2. The systematic uncertainties on the ratios for all targets and Q^2 are presented in Table I.

Q^2	1.55	1.85	2.15	2.45
δR^A	7.1	5.8	4.9	5.1
δR^{He4}	0.7	0.7	0.7	0.7

TABLE I: Systematic uncertainties δR^A and δR^{He4} for the ratio of normalized inclusive yields $R^{C,Fe}_{^3He}$ and $R^{^4He}_{^3He}$ respectively, in %. Q^2 in (GeV/c)^2, and $\Delta Q^2 = \pm 0.15$ (GeV/c)^2.

B. Probabilities of 2-Nucleon Short Range Correlations in Nuclei

Our data are clearly consistent, both qualitatively and quantitatively, with the predictions of the NN SRC model. The obtained (averaged for $1.4 < Q^2 < 2.6$ (GeV/c)^2 region) ratios, $R^A_{^3He}$, are shown in Table 2 as a function of x_B. Fig. 9 shows these ratios for the ^{12}C and ^{56}Fe targets together with the SRC calculation by [10]. Good agreement between data and calculation is seen.

Experimental data in the scaling region can be used to estimate the relative probabilities of NN SRC in nuclei compared to ^{3}He. According to [1] the ratio of these probabilities are proportional to the ratio defined as:

$$r^A_{^3He} = \frac{(2\sigma_p + \sigma_n)\sigma_A}{(Z\sigma_p + N\sigma_n)\sigma_{3He}} \quad (8)$$

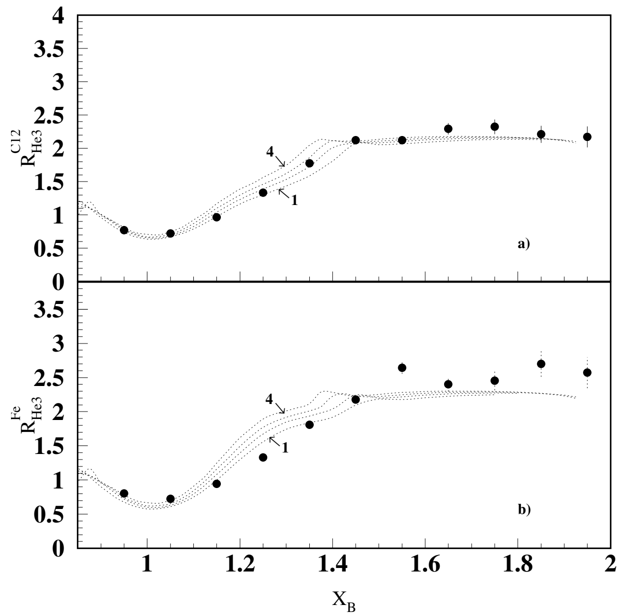

FIG. 9: $R^A_{^3He}(x_B)$ as a function of x_B for 1.4<Q^2 <2.6 (GeV/c)^2. Curves are SRC model predictions: 1 and 4 - at Q^2=1.4 and 2.6 (GeV/c)^2, respectively. a) ^{12}C, b) ^{56}Fe.

where σ_A and σ_{3He} are the $A(e,e')$ and $^3\text{He}(e,e')$ inclusive cross sections respectively. σ_p and σ_n are the electron-proton and electron-neutron elastic scattering cross sections respectively. Z and N are the number of protons and neutrons in nucleus A. Using Eq.(4) the ratio of Eq.(8) can be related to the experimentally measured ratios $R^A_{^3He}$ as

$$r^A_{^3He} = R^A_{^3He}(x_B, Q^2) \times \frac{A(2\sigma_p + \sigma_n)}{3(Z\sigma_p + N\sigma_n)} \quad (9)$$

X_B	^{4}He	^{12}C	^{56}Fe
0.95 ± 0.05	0.86 ± 0.004	0.77 ± 0.003	0.80 ± 0.004
1.05 ± 0.05	0.78 ± 0.004	0.72 ± 0.003	0.72 ± 0.004
1.15 ± 0.05	0.94 ± 0.006	0.96 ± 0.006	0.94 ± 0.007
1.25 ± 0.05	1.19 ± 0.012	1.33 ± 0.012	1.33 ± 0.015
1.35 ± 0.05	1.41 ± 0.021	1.77 ± 0.025	1.81 ± 0.030
1.45 ± 0.05	1.58 ± 0.033	2.12 ± 0.044	2.17 ± 0.055
1.55 ± 0.05	1.71 ± 0.049	2.12 ± 0.059	2.64 ± 0.087
1.65 ± 0.05	1.70 ± 0.063	2.29 ± 0.085	2.40 ± 0.109
1.75 ± 0.05	1.85 ± 0.089	2.32 ± 0.110	2.45 ± 0.139
1.85 ± 0.05	1.65 ± 0.100	2.21 ± 0.128	2.70 ± 0.190
1.95 ± 0.05	1.71 ± 0.124	2.17 ± 0.157	2.57 ± 0.227

TABLE II: The measured ratios, $R^A_{^3He}$, averaged for $1.4 < Q^2 < 2.6$ (GeV/c)^2 interval.

To obtain the numerical values for $r^A_{^3He}$ we calculated the second factor in Eq. (9) using parameterizations for

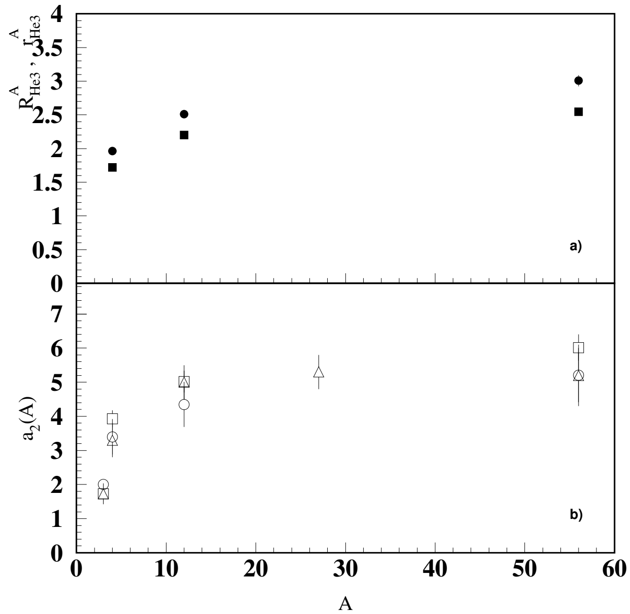

FIG. 10: a) $R^A_{^3He}$ (■) and $r^A_{^3He}$ (•) versus A.
b) $a_2(A)$ versus A. ∘ - $a_2(A)$ is calculated from Eq.(10) using the experimental value of $a_2(3)$ Ref. [5]; □ - $a_2(A)$ is calculated using the theoretical value of $a_2(3)$; △ - data from Ref. [5].

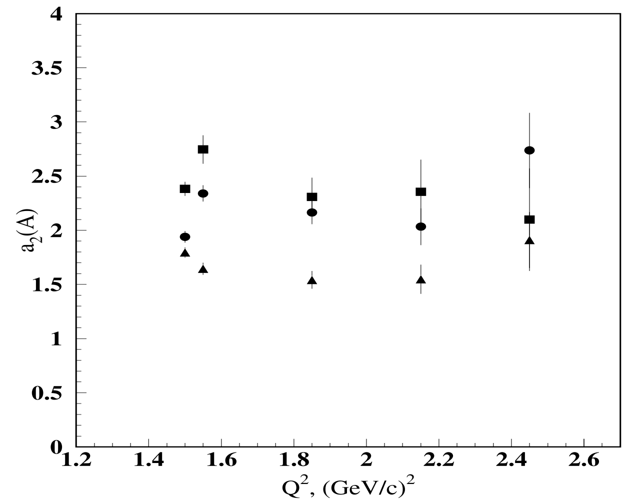

FIG. 11: Q^2 - dependences of $a_2(A)$ parameters for target-nuclei ^{4}He (▲)) , ^{12}C (•) and ^{56}Fe (■).

	$R^A_{^3He}(x_B)$	$r^A_{^3He}$	$a_2(A)^{exp}$	$a_2(A)^{theor}$
^{4}He	1.72 ± 0.03	1.96 ± 0.05	3.39 ± 0.51	3.93 ± 0.24
^{12}C	2.20 ± 0.04	2.51 ± 0.06	4.34 ± 0.66	5.02 ± 0.31
^{56}Fe	2.54 ± 0.06	3.00 ± 0.08	5.21 ± 0.79	6.01 ± 0.38

TABLE III: $R^A_{^3He}(x_B)$ is the ratio of normalized (e, e') yields for nucleus A to ^{3}He. $r^A_{^3He}$ is the relative per-nucleon probability of SRC for the two nuclei. Both values are obtained from the scaling region ($Q^2 > 1.4$ and $x_B > 1.5$). $a_2(A)^{exp}$ and $a_2(A)^{theor}$ are the $a_2(A)$ parameters obtained by multiplying $\frac{a_2(A)}{a_2(3)}$ with the experimental and theoretical values of $a_2(3)$, respectively. The $R^A_{^3He}(x_B)$ ratios include statistical errors only. Errors of $r^A_{^3He}$ include also uncertainties in the second factor in Eq.(9). Errors in $a_2(A)^{exp}$ and $a_2(A)^{theor}$ also include uncertainties in the corresponding values of $a_2(3)$. For systematic uncertainties see Table I. There is an overall theoretical uncertainty of 20% in converting these ratios into SRC probabilities.

the neutron and proton form factors [27–30]. We found the average values of these factors to be 1.14 ± 0.02 for ^{4}He and ^{12}C, and 1.18 ± 0.02 for ^{56}Fe. Note that these factors vary slowly over our Q^2 range. For $r^A_{^3He}$ calculations the experimental data were integrated over $Q^2 > 1.4$ (GeV/c)^2 and $x_B > 1.5$ for each nucleus. The ratio of integrated yields, $R^A_{^3He}(x_B)$, are presented in the first column of Table III and in Fig. 10a (rectangles). The ratios $r^A_{^3He}$ are shown in the second column of Table III and by the circles in Fig. 10a. One can see that the ratios $r^A_{^3He}$ are 2.5 - 3.0 for ^{12}C and ^{56}Fe, and approximately 1.95 for ^{4}He.

The per-nucleon SRC probability in nucleus A relative to ^{3}He is proportional to $r^A_{^3He} \sim a_2(A)/a_2(3)$, where $a_2(A)$ and $a_2(3)$ are the per-nucleon probability of SRC relative to deuterium for nucleus A and ^{3}He. As was discussed earlier, the direct relation of $r^A_{^3He}$ to the per-nucleon probabilities of SRC has an uncertainty of up to 20% due to pair center of mass motion. Within this uncertainty, we will define the per-nucleon SRC probabilities of nuclei relative to deuterium as:

$$a_2(A) \ = \ r^A_{^3He} \cdot a_2(3) \qquad (10)$$

Two values of $a_2(3)$ have been used to calculate $a_2(A)$. First is the experimentally obtained value from [5], $a_2(3) = 1.7 \pm 0.3$, and the second the value from the calculation using the wave function for deuterium and ^{3}He, $a_2(3) = 2 \pm 0.1$. Similar results were obtained in Ref. [31].

The per-nucleon probability of SRC for nucleus A relative to deuterium is shown in the third and fourth columns of Table III and in Fig. 10b. The uncertainties in existing $a_2(3)$ are included in the errors for $a_2(A)$. The results from [5] are shown as well. One can see that $a_2(A)$ changes significantly from $A = 4$ to $A = 12$ but does not change significantly for $A \geq 12$. There are approximately 5.5 times as much SRC for $A \geq 12$ than for deuterium, and approximately 3.5 times as much SRC for ^{4}He as for deuterium. These results are consistent with the analysis of the previous SLAC (e, e') data [5]. They are also consistent with calculations of Ref. [31].

Fig. 11 shows the Q^2 dependence of the relative SRC probability, $a_2(A)$ which appears to be Q^2 independent for all targets.

V. SUMMARY

The $A(e,e')$ inclusive electron scattering cross section ratios of ^{4}He, ^{12}C, and ^{56}Fe to ^{3}He have been measured for the first time under identical conditions.

It is shown that:

1. These ratios are independent of x_B (scale) for $x_B > 1.5$ and $Q^2 > 1.4$ (GeV/c)^2 for high recoil momentum. The ratios do not scale at $Q^2 < 1.4$ (GeV/c)^2.
2. These ratios in the scaling region are:
   - independent of Q^2.
   - approximately independent of A for $A \geq 12$.
3. These features were predicted by the Short Range Correlation model of inclusive $A(e,e')$ scattering at large x_B [5].
4. The observed scaling shows that the momentum distributions at high momenta have the same shape for all nuclei and differ only by a scale factor.
5. Using the SRC model, the values of the ratios in the scaling region were used to derive the relative probabilities of SRC in nuclei compared to deuterium. The per-nucleon probability of Short Range Correlations in nuclei relative to deuterium is ≈ 3.5 times larger for ^{4}He and 5.0 - 5.5 times larger for ^{12}C and ^{56}Fe.

ACKNOWLEDGMENT

We acknowledge the efforts of the staff of the Accelerator and Physics Divisions (especially the Hall B target group) at Jefferson Lab in their support of this experiment. This work was supported in part by the U.S. Department of Energy, including DOE Contract No. DE-AC05-84ER40150, the National Science Foundation, the French Commissariat a l'Energie Atomique, the Italian Istituto Nazionale di Fisica Nucleare, and the Korea Research Foundation. We also acknowledge useful discussions with D. Day and E. Piasetzki.

[1] L.L. Frankfurt and M.I. Strikman, Phys. Rep. **76**, 215 (1981); **160**, 235 (1988).
[2] T.W. Donnelly and Ingo Sick, Phys. Rev. C **60**, 065502 (1999);
J. Arrington, *et al.*, Phys. Rev. Lett. **82**, 2056 (1999).
[3] C. Ciofi degli Atti, Phys.Rev. C**53**, 1689, (1996).
[4] L.Frankfurt and M. Strikman, in *Electromagnetic Interactions with Nuclei*, edited by B. Frois and I. Sick (World Scientific, Sngapore, 1991).
[5] L.L. Frankfurt, M.I. Strikman, D.B. Day, M.M. Sargsyan, Phys. Rev. C **48**, 2451, (1993).
[6] W.P. Schutz *et al.*, Phys. Rev. Lett. **38**, 8259 (1977).
[7] S. Rock *et al.*, Phys. Rev. Lett. **49**, 1139 (1982).
[8] R.G. Arnold *et al.*, Phys. Rev. Lett. **61**, 806 (1988).
[9] D. Day *et al.*, Phys. Rev. Lett. **59**, 427 (1979).
[10] M. Sargsian, CLAS-NOTE 90-007 (1990).
[11] M.V. Zverev and E.E. Saperstein, Yad. Fiz. **43**, (1986) 304.
[12] A. Bodek *et al.*, Phys. Rev. D **20**, (1979) 1471.
[13] D. Day *et al.*, Phys. Rev. Lett. **43**, (1979) 1143.
[14] Th.C. Petitjean, Inagural-Dissertation, Basel, 2000.
[15] L. L. Frankfurt, M. M. Sargsian and M. I. Strikman, Phys. Rev. C **56**, 1124 (1997).
[16] M.M. Sargsian, Dissertation, Yerevan, 1993 and Int. J. Mod. Phys. E **10**, 405 (2001).
[17] C. Ciofi degli Atti, S. Simula, L. L. Frankfurt and M. I. Strikman,Phys. Rev. C **44**, 7 (1991).
[18] C. Ciofi degli Atti, Private Communication.
[19] O. Benhar, A. Fabrocini, S. Fantoni, G. A. Miller, V. R. Pandharipande and I. Sick, Phys. Rev. C **44**, 2328 (1991).
[20] O. Benhar, A. Fabrocini, S. Fantoni and I. Sick, Phys. Lett. B **343**, 47 (1995).
[21] K. Garrow *et al.*, arXiv:hep-ex/0109027.
[22] CEBAF Hall B Conceptual Design Report, April 1990.
[23] M.D. Mestayer *et al.*, Nucl. Inst. and Meth. **A449**, 81 (2000).
[24] E.S. Smith *et al.*, Nucl. Inst. and Meth. **A432**, 265 (1999).
[25] G. Adams *et al.*, Nucl. Inst. and Meth. **A465**, 414 (2001).
[26] M. Amarian *et al.*, Nucl. Inst. and Meth. **A460**, 239 (2001).
[27] I.G. Aznauryan, Private Communication.
[28] Kees De Jager, JLAB-PHY-00-01, 2001.
[29] P.E. Bosted *et al.*, Phys. Rev C **51**, (1995) 409.
[30] M.L. Miller *et al.*, Phys. Rev. Lett. **84**, (2000) 1398.
[31] J.L. Forest *et al.*, Phys. Rev. C **54**, (1996) 646.
[32] Hereafter, by the ratio of the cross sections we will mean the ratios weighted by A. We will separately discuss effects due to $\sigma_{ep} > \sigma_{en}$ which are important for ^{3}He due to Z not equal to N.
[33] So far no color transparency effects are observed in $A(e,e'p)X$ reactions at $Q^2 \leq 8$ (GeV/c)^2, [21]